Density Functional Theory Studies of Chemisorption and Diffusion Properties of Ni and Ni−Thiophene Complexes on the MoS_2 Basal Plane

Dan C. Sorescu,*,†,‡ David S. Sholl,†,§ and Anthony V. Cugini†

U.S. Department of Energy, National Energy Technology Laboratory, P.O. Box 10940, Pittsburgh, Pennsylvania 15236, Department of Chemical and Petroleum Engineering, University of Pittsburgh, Pittsburgh, Pennsylvania 15261, and Department of Chemical Engineering, Carnegie Mellon University, Pittsburgh, Pennsylvania 15213

Received: May 21, 2002

First principles calculations based on spin-polarized density functional theory and the generalized gradient approximation have been used to study the chemisorption and diffusion of Ni atoms and clusters and a Ni−thiophene complex on defect-free MoS_2(0001). The calculations employ slab geometry and periodic boundary conditions. We have identified several possible adsorption configurations of Ni atoms on the surface. The most stable configuration corresponds to adsorption at 3-fold hollow sites. By increasing the Ni coverage, several types of clusters can be formed that have a lower binding energy per Ni atom than single adsorbed Ni atoms. Minimum energy pathways for the diffusion of Ni atoms between selected pairs of local minima have been determined. The results indicate the existence of relatively large barriers for hopping with values between 20 and 44 kcal/mol. Additional calculations have been performed to analyze the adsorption of the thiophene molecule on bare and Ni-covered MoS_2 basal planes. Ni atoms significantly increase the adsorption energy of thiophene up to 21 kcal/mol. However, the diffusion barrier of the Ni−thiophene complex between 3-fold sites remains high with a value of 21.2 kcal/mol. Finally, the role of sulfur defects upon the chemisorption of Ni atoms has been investigated. These defects further stabilize the Ni atoms on the surface and slightly decrease the binding energy of thiophene on these metallic atoms.

I. Introduction

The production of clean fuels by hydrotreating and hydrodesulfurization (HDS) is an area of major research interest due to the new environmental legislation regarding fuel specifications. The EPA's new Tier 2 Clean Air Standards state that the content of sulfur in gasoline should be reduced to 30 ppm by 2006 from the current level of 300 ppm.[1] Among different technological approaches taken to achieve these goals, improving the efficiency of HDS is a key issue. In particular, it is necessary to remove both the readily destroyed sulfur compounds as well as the complement sulfur species that are not eliminated with the current technologies.

Among various metal sulfide catalysts proposed for HDS, molybdenum disulfide (MoS_2) is one of the most promising candidates for petroleum-refining industries.[2,3] In practice, it is used as well-dispersed MoS_2 nanocrystallites supported on γ-alumina and can be used both as an unpromoted or promoted catalyst[2] with Co or Ni promoter atoms. In the case of unpromoted catalysts, experimental studies[3,4] have indicated that the main activity is at the edges of the MoS_2 clusters where sulfur vacancies are created. It is generally believed that sulfur-containing molecules cannot adsorb on completely sulfided catalysts; consequently, sulfur vacancies have to be created to provide catalytic activity.

The performance of the MoS_2 catalysts for HDS can be significantly improved by the use of metallic promoters where the Co−Mo−S and Ni−Mo−S structures are responsible for the catalytic activity.[2−4] In this case, the identification of the role played by Co or Ni promoter species as well as the location of these species on the MoS_2 surface has attracted significant interest in recent years from both experimental and theoretical groups.[3,5−10] In particular, important insight has emerged from the STM investigations of model HDS catalysts performed by Besenbacher and co-workers.[5,6] They have shown that in the case of MoS_2 nanoclusters deposited on the Au(111) surface the MoS_2 clusters change their shape from a triangular to a truncated hexagonal configuration in the presence of Co. Co atoms were found preferentially to be located at the S edge of MoS_2 clusters. At this edge, Co atoms appear to substitute into Mo positions where they induce an enhanced electronic density at the nearby S atoms.

Additional STM work performed by Weiss and co-workers[10−12] has focused on the description of the dynamics of Ni and Co clusters on MoS_2 basal planes. On the basis of low-temperature scanning tunneling microscopy investigations, they have indicated that both of these species have a low barrier for diffusion. At temperatures as low as 4 K, Ni clusters ranging in size from a few atoms to larger islands were observed. It was suggested that these promoters could be used to increase the sticking probability of sulfur-containing hydrocarbons and to transport these hydrocarbons to the active sites for reaction. These experiments raise several issues that are not yet fully understood. For example, the location of the promoters on the basal plane or the electronic modifications induced upon the adsorption of these metallic atoms is not yet well established. Moreover, the transport properties, particularly the diffusion and clustering characteristics of these promoters on MoS_2, have not been yet

* Corresponding author. E-mail: sorescu@pp.netl.doe.gov.
† U.S. Department of Energy.
‡ University of Pittsburgh.
§ Carnegie Mellon University.

10.1021/jp021251s CCC: $25.00
Published on Web 01/31/2003

fully characterized. These experiments also hint at the role played by sulfur defects on the chemisorption properties of promoter atoms. It would be useful to understand how the adsorption and dissociation of various hydrocarbon species containing sulfur are changed in the presence of the promoters and of the sulfur vacancies on MoS_2.

Interactions of thiophene with MoS_2 basal surfaces have been examined in several experiments.[13,14] Thiophene was found to adsorb very weakly on the MoS_2 (0001) surface and desorbed molecularly at 165 K. By assuming a preexponential factor of 10^{13} s^{-1}, a binding energy of 9.5 kcal/mol was estimated.[13] Rodriguez et al.[14] investigated the adsorption of thiophene on clean and Ni-promoted MoS_x using synchrotron-based high-resolution photoemission. Their results confirm the existence of a weak chemisorption of thiophene on MoS_x surfaces with a desorption temperature around 200 K. The presence of S vacancies on the surface slightly increased the binding energy of molecules, as indicated by the increase of the desorption temperature up to 300 K. In the presence of Ni promoters, the chemical activity of the surface increases, and the adsorption energy of thiophene is found to be at least 5−10 kcal/mol larger than on pure MoS_x. However, it was observed that the presence of Ni adatoms is not enough to promote the cleavage of C−S bonds.

The first step to describe theoretically the interaction of Ni atoms with MoS_2 basal planes was made by Rodriguez.[15] Using INDO/S and unrestricted Hartree−Fock calculations in conjunction with cluster models representing MoS_2(0001) and MoS_2-$(10\bar{1}0)$ surfaces, it was determined that a significant reduction (0.5−2 eV) in the stability of the HOMOs takes place upon Ni adsorption. On the basal plane, it was found that H_2 and thiophene molecules are only weakly bound but the binding energy is increased when Ni atoms are present on the surface. These results suggest that one role played by Ni when adsorbed on the basal MoS_2 surface is to enhance the chemical activity of this surface by providing sites for the chemisorption of thiophene.

More recently, the properties of promoted MoS_2 catalysts have been also analyzed using more accurate theoretical methods such as density functional theory (DFT).[5,9,16−19] In a series of papers, Raybaud et al.[9,16] have investigated the binding and electronic properties of the promoter species at the $(10\bar{1}0)$ surface (Mo-edge plane) and the $(\bar{1}010)$ surface (S-edge plane) where the catalytic activity is the highest. In a subsequent study, Raybaud et al.[17] have analyzed a number of intercalation and pseudo-intercalation configurations in which the promoter atoms interact with the MoS_2 basal plane inside the van der Waals gap. It was found that the most favorable configuration corresponds to a tetrahedral pseudointercalated position where the promoter is 4-fold coordinated by sulfur atoms and has one molybdenum neighbor. In the same study,[15] the substitution of one of the molybdenum edge sites with a promoter atom has also been investigated, and it has been determined that this leads to a significant stabilization of about 1.7 eV per cell in comparison to the pseudointercalation configuration.

The influence of the practical conditions of temperature and pressure used in HDS processes upon the equilibrium S coverage of the active edges has also been analyzed by Raybaud et al.[18,19] They have shown that the chemical potential of S, which depends on temperature and the pressure ratio of H_2S and H_2 species, has a direct influence on the shape of the MoS_2 crystallite and the local edge structure. For the most stable clusters determined, the STM simulated images were found[19] to be in qualitatively good agreement with the experimental data of Helveg et al.[6]

In an attempt to clarify some of the issues raised by the STM work of Weiss et al.[11] related to the structural and binding properties of Ni atoms on the MoS_2 basal plane, we report in this study the results of first principles DFT calculations within the pseudopotential approximation for this particular system. The periodic nature of the surface, which is neglected in simple cluster models, has been considered here by using a tridimensional slab model (supercell model) repeated periodically in all three directions. Beside a description of the geometric and energetic properties of Ni atoms and clusters adsorbed at various sites on MoS_2(0001), we also report the adsorption properties of thiophene on the surface with preadsorbed Ni atoms. We further analyze the corresponding chemisorption properties for the case of a surface with sulfur defects. Finally, we analyze the minimum-energy potential path for the diffusion of Ni and Ni−thiophene complexes between different adsorption sites. We emphasize that the main aim of our work, as in the experiments of Weiss et al., is to examine the fundamental mechanisms of Ni adsorption and diffusion on MoS_2 basal planes, not to directly examine the full range of surface species and catalytically active edge sites that exist under practical HDS conditions.

The organization of the paper is as follows. In section II, we describe the computational methods. The results of total energy calculations for the adsorption of Ni atoms, Ni clusters, thiophene, and Ni−thiophene complexes as well as for the description of the minimum-energy pathways between different equilibrium configurations are given in section III. Finally, we summarize the main conclusions in section IV.

II. Computational Method

Our calculations were made using the ab initio total-energy program VASP (Vienna ab initio simulation program) and the ultrasoft pseudopotential database contained therein.[20−22] This work has been performed using the spin-polarized PW91 generalized gradient approximation (GGA) of Perdew et al.[23] This program evaluates the total energy of periodically repeating geometries on the basis of density-functional theory and the pseudopotential approximation. In this case, the electron−ion interaction is described by fully nonlocal optimized ultrasoft pseudopotentials (USPs) similar to those introduced by Vanderbilt.[24,25] Periodic boundary conditions are used, with the one-electron pseudo-orbitals expanded over a plane wave basis set. The expansion includes all plane waves whose kinetic energy is less than a predetermined cutoff energy E_{cut}. A cutoff energy of 242 eV has been used in our studies. The Brillouin zone was sampled with the lowest-order Monkhorst−Pack[26] set of one k point for geometric optimizations and nine k points for calculations of the densities of states. In a number of instances, we have tested the accuracy of PW91 results using the projector augmented wave (PAW) method.[27,28] In this case, a cutoff energy of 400 eV has been used. Electron smearing is employed via the Gaussian or Methfessel−Paxton technique,[29,30] with a smearing width of $\sigma = 0.1$ eV. The optimization of different atomic configurations is based upon a conjugate-gradient minimization of the total energy, using the Hellmann−Feynman forces on the atoms.

Minimum-energy paths between different minima were optimized by use of the nudged elastic band (NEB) method of Jónsson and co-workers.[31] In this approach, the reaction path is "discretized", with the discrete configurations, or images, between minima being connected by elastic springs to prevent

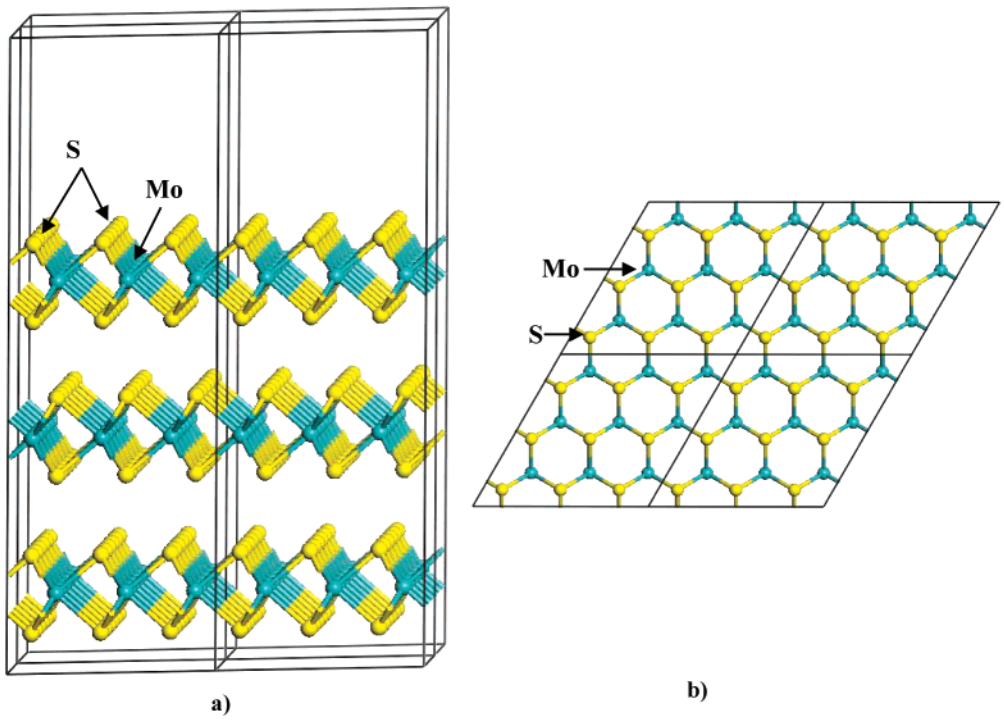

Figure 1. (a) Side and (b) top views of the $MoS_2(0001)$ slab model with three S−Mo−S trilayers.

the images from sliding to the minima in the optimization. In the NEB searches, either 8 or 16 images were employed between minima.

III. Results and Discussion

A. Calculations for Bulk MoS_2. A number of tests have been performed to benchmark the accuracy of our DFT calculations by examining bulk MoS_2. To determine the equilibrium bulk parameters of MoS_2, we minimized the total energy with respect to the volume and shape of the unit cell and the atomic coordinates within the experimentally determined space group symmetry. For the experimental structure of MoS_2, we have used the X-ray data reported by Bronsema et al.,[32] who reported that the crystal is hexagonal within the $P6_3/mmc$ space group with lattice dimensions of $a = 3.1602$ Å and $c = 12.294$ Å. The atoms are positioned at coordinates 2c $\{\pm(^1/_3, ^2/_3, ^1/_4)\}$ for Mo and 4f $\{\pm(^1/_3, ^2/_3, z; ^1/_3, ^2/_3, ^1/_2 - z), z = 0.621\}$ for S atoms, respectively. Our calculations give lattice dimensions of $a_{calc} = 3.1723$ Å and $c_{calc} = 12.6212$ Å, which differ by 0.38% and 2.66% from the experimental data with an axial ratio of $^c/_a = 3.97$ ($^c/_{a(exp)} = 3.89$) and a volume ratio of $V_{calc}/V_{exp} = 1.034$. The internal parameter, z, is found in our calculations to be 0.625. For the crystallographic parameters found in our calculations, the S−S first neighbor distances within the S−Mo−S trilayer (see Figure 1) are found to be equal to 3.13 Å whereas the interlayer distances are 3.66 Å. These values should be compared against the experimental values of 3.17 and 3.49 Å, respectively. Similarly, the covalent Mo−S distance is predicted to be 2.41 Å whereas the corresponding experimental value is 2.42 Å. It is important to note that the weak interactions between successive S−Mo−S trilayers in MoS_2 represent a challenge for DFT calculations since these methods do not quantitatively represent dispersion interactions. As a consequence, the interlayer spacings are predicted with less accuracy in our calculations than the other structural parameters. These results are in very close agreement with those reported previously by Raybaud et al.[33] using a computational method similar to the one described in this work.

From an electronic point of view, bulk MoS_2 is a semiconductor. This has been shown previously by Raybaud et al.[33] on the basis of the calculated band structure and density of states (DOS) for the bulk crystal. We have repeated these calculations and have found that the band gap is about 1 eV, in good agreement with previous findings of Raybaud et al.[33]

B. Slab Calculations for the $MoS_2(0001)$ Surface. As noted above, the existence of weak interactions between successive S−Mo−S sheets represents a challenge for DFT predictions. To test the accuracy of our methods for predicting the geometric parameters of the $MoS_2(0001)$ surface, we investigated slab models with different numbers of layers. In particular, we constructed surface supercells containing 3×3 surface units with one and three S−Mo−S trilayers. Figure 1 shows the supercell used in the latter case. The total number of atoms is 9 Mo and 18 S in the first case and 27 Mo and 54 S in the second case. A vacuum width of about 11 Å has been chosen. For the surface slab with one trilayer, the results of full atomic relaxations indicate very small changes relative to the bulk structure. For example, the Mo−S and S−S distances inside the trilayer are 2.41 and 3.12 Å, respectively, practically identical to the values obtained for the optimized bulk structure. A similar conclusion is reached for the case when there are three trilayers in the surface slab. However, in this last case, we observed the increase of the separation between the neighboring trilayers in a direction perpendicular to the surface normal. As a result, the interlayer S−S separation increases from 3.66 Å, corresponding to a bulk value to 4.32 Å. These rather large displacements indicate the difficulty of the DFT method in accurately reproducing the weak van der Waals interactions present between MoS_2 layers. However, it is important to note that because of the relatively large separation between the neighboring trilayers it is expected that there will be only a small influence of the chemisorption properties of molecules on top of the (0001) surface from the subsurface layers. Consequently, in the majority of studies performed in the present work, we limited ourselves to a slab model containing a single trilayer. In a few instances, however, we have further tested the results

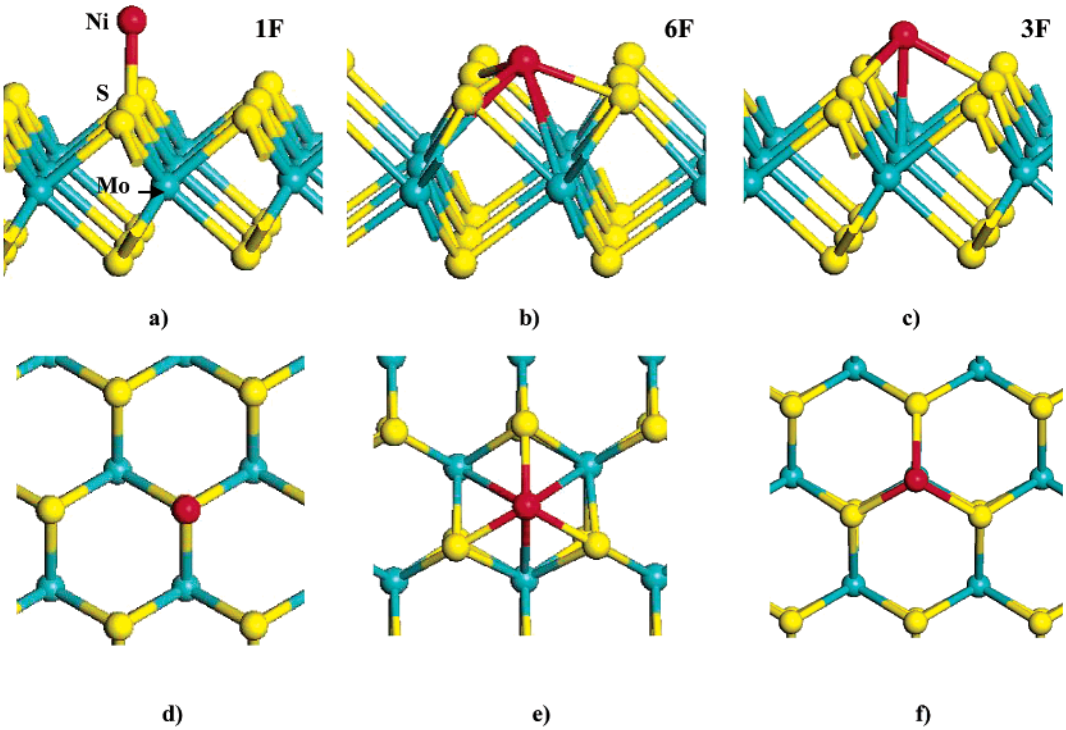

Figure 2. Pictorial representation of the lateral and top views of the adsorption configurations of Ni on the MoS_2(0001) surface: (a) on top of sulfur atoms (1F), (b) 6-fold configuration (6F), and (c) 3-fold configuration (3F).

using a three-trilayer slab model in which the interlayer spacing was constrained to the optimized bulk value. As will be shown below, the corresponding results are not influenced by this choice.

C. Test Calculations for the Isolated Thiophene Molecule. As one of the goals of the present work is to describe the chemisorption of thiophene on either a bare or a Ni-covered MoS_2 (0001) surface, it is important to check the correspondence to theoretical predictions for the case of this molecule in the gas phase. Such calculations have been previously made by Raybaud et el.[9] in connection with the adsorption studies of thiophene on the catalytically active MoS_2(010) surface. We have verified their results by optimizations of an isolated thiophene molecule placed in a cubic box of side 10 Å. The predicted C−C, C═C, and C−S bond lengths were found to be accurate within 1.0% of the corresponding experimental data[34,35] whereas the deviation found for C−H bonds from experimental data is about 1.3%. Similar agreement is seen for the corresponding bond angles.

The good performances of the set of Ni pseudopotentials provided in the VASP program to describe the bulk properties of Ni have been analyzed in great detail by Moroni et al.[36] and will not be repeated here. Overall, the good agreement of the calculated results for bulk MoS_2, the bare MoS_2(0001) surface, and gas-phase thiophene with experimental data made us confident to proceed to the next step (i.e., the investigation of the chemisorption properties of Ni species and the thiophene molecule on the MoS_2(0001) surface).

D. Ni Adsorption on the MoS_2(0001) Surface. D1. Single Atom Adsorption. As indicated above, the majority of calculations for the adsorption of Ni atoms on the MoS_2 (0001) surface have been made using a 3 × 3 slab with one S−Mo−S trilayer containing a total of 9 Mo and 18 S atoms. For each configuration, the adsorption energy can be defined by

$$E_{ads} = \{NE_{Ni} + E_{slab} - E_{(ads+slab)}\}/N \qquad (1)$$

where E_{Ni} is the energy of an isolated spin-polarized Ni atom, E_{slab} is the total energy of the slab in the absence of the adsorbate, $E_{(ads+slab)}$ is the total energy of the adsorbate/slab system, and N is the total number of Ni atoms in the supercell. A positive E_{ads} corresponds to a stable adsorbate/slab system. However, as the energy of the Ni atom is likely to be poorly reproduced by DFT calculations, an alternative evaluation of the binding energies can be made with respect to the energy of the most stable adsorption site for an isolated Ni atom on the surface: $E_{rel} = E_{ads} - E_{ads,0}$, where $E_{ads,0}$ represents the reference state. With this definition, a negative value of E_{rel} corresponds to a state that is less stable on the surface than the reference state.

On the basis of full geometry optimizations of the Ni atom on the MoS_2 basal plane, we have considered three adsorption configurations for isolated Ni atoms. The first one, denoted 1F (see Figure 2a), corresponds to a Ni atom adsorbed on top of the sulfur atoms. As will be shown in a next section, this configuration actually corresponds to a saddle point rather than a local minimum. The second one, denoted 6F, corresponds to a 6-fold hollow site (see Figure 2b) in which a Ni atom is surrounded by three Mo and three S atoms. The last one, denoted 3F, corresponds to adsorption on top of a Mo atom with 3-fold binding to neighboring sulfur atoms (see Figure 2c). The corresponding geometric and energetic parameters for these configurations are given in Table 1.

As indicated in section (a) of Table 1, our results indicate a stability order of E_{ads}(3F) > E_{ads}(6F) > E_{ads}(1F). For the most stable adsorption configuration, 3F, the adsorption energy using eq 1 is about 77 kcal/mol. In this configuration, the Ni atom binds simultaneously to both the Mo atom directly beneath it and three neighboring S atoms. The corresponding Ni−Mo and Ni−S separations are 2.59 and 2.12 Å, respectively. For the other two binding configurations, similar Ni−S separations are found (see Table 1).

TABLE 1: Calculated Equilibrium Distances and the Adsorption Energies for Various Atomic Configurations Considered in the Present Study[a]

config.[b]	θ[c]	r(Ni−S)[d]	r(Ni−Mo)	E_{rel}[f]	config.	θ[c]	r(Ni−S)[e]	r(Ni−Mo)[e]	E_{rel}[f]
(a) USP, Slab with One Trilayer					(c) PAW, Slab with One Trilayer				
1F	1/9	1.969	4.006	−43.7	1F	1/9	1.958	3.991	−40.0
6F	1/9	2.066	2.864	−10.6	6F	1/9	2.067	2.819	−8.6
3F	1/9	2.123	2.590	0.0	3F	1/9	2.121	2.581	0.0
(b) USP, Slab with Three Trilayers									
1F	1/9	1.974	3.984	−44.6					
6F	1/9	2.075	2.836	−9.6					
3F	1/9	2.126	2.587	0.0					

config.	θ[c]	r(Ni−S)[e]	r(Ni−Mo)[e]	r(Ni−Ni)[e]	E_{rel}	$E_{ads,g}$[g]
(d) USP, Slab with One Trilayer						
1F−1F	2/9	2.085	3.832	2.240	−31.5	
6F−6F	2/9	2.082	2.797	2.916	−9.8	
1F−6F	2/9	2.097	3.001	2.420	−21.8	
1F−3F	2/9	2.114	2.629	2.409	−16.1	
6F−3F	2/9	2.101	2.671	2.296	−7.8	
3F−3F	2/9	2.126	2.628	3.123	0.0	0.4
3F sites	3/9	2.131	2.663	3.168		0.9
3F sites	4/9	2.136	2.692	3.144		1.1
3F sites	5/9	2.150	2.726	3.024		1.6
3F sites	6/9	2.148	2.722	3.039		2.4
3F sites	7/9	2.146	2.710	3.086		2.8
3F sites	8/9	2.151	2.732	3.096		3.1
3F sites	9/9	2.161	2.766	3.162		3.4

config.[h]	r(Ni−Mo)	r(Ni−S_{th})	r(S_{th}−C)	r(C═C)	r(C−C)	E_{ads}
(e) USP, Slab with One Trilayer						
TH(v) + Ni	2.635	2.195	1.722	1.373	1.427	19.4
TH(h) + Ni	2.640	2.248	1.743	1.366	1.436	21.1
(f) PAW, Slab with One Trilayer						
TH(v) + Ni	2.634	2.203	1.724	1.368	1.430	18.9
TH(h) + Ni	2.628	2.233	1.738	1.365	1.432	20.0

[a] Sections a−d refer to the Ni atom and Ni clusters adsorbed on MoS_2(0001) at different surface sites and for different coverages θ. Sections e and f correspond to the thiophene molecule adsorbed on top of the Ni atom positioned at 3F sites. The results are differentiated for the case of ultrasoft pseudopotentials (USP) and the projector augmented wave (PAW), respectively. All lengths and energies are shown in angstroms and kcal/mol, respectively. [b] Notations 1F, 6F, and 3F correspond to the adsorption on top of S atoms, in 6-fold, and in 3-fold configurations, respectively. The mixed notations 1F−3F, 1F−6F, 1F−3F, 1F−1F, 3F−3F, and 6F−6F indicate the type of surface sites where the adsorption of Ni dimers takes place. [c] We define $\theta = 1$ to be an adlayer in which there is one Ni adatom per Mo atom in the top trilayer. [d] The indicated bond distances correspond to the average over equivalent bonds. [e] The indicated bond distances correspond to the minimum value among the entire set of different distances. [f] The indicated relative adsorption energies E_{rel} are given with respect to the adsorption at the most stable 3F site. [g] This energy has been determined on the basis of eq 2 described in text. [h] The adsorption configurations of thiophene (TH) on top of the Ni atom correspond to a vertical configuration through the S end (v) and, respectively, a configuration with the aromatic ring lying along the surface (h).

We have checked the sensitivity of our results against the number of trilayers in the slab. For this purpose, we used a slab with three trilayers and with two atoms adsorbed on the opposite faces of the slab. The corresponding results are indicated in section (b) of Table 1. In this case, the adsorption energies and geometric parameters for all surface sites are practically unchanged relative to the case when a single trilayer slab has been used. These results indicate that the use of the slab with a single S−Mo−S trilayer is sufficiently accurate to determine the corresponding adsorption parameters. Consequently, in all of our following calculations, we have used a single-trilayer slab model.

Finally, we have analyzed the modifications of the present set of results for the case of the projector augmented wave (PAW) method, shown to provide an accurate description of the chemisorption properties of molecules on surfaces.[37−39] As indicated in section (c) of Table 1, the geometrical parameters obtained using the PAW method are very close to those determined on the basis of ultrasoft pseudopotentials. The relative stability order among the three adsorption sites is also maintained for this method, but the adsorption energies are slightly larger than those obtained using USPs. Overall, the two methods provide similar data on the energetic and geometric parameters of Ni atoms adsorbed at various sites on the MoS_2 surface.

It is useful to compare the preference for the 3F adsorption site seen in this study with findings from other similar experimental or theoretical studies. Weiss et al.[12] have shown in their STM investigations that on the defect-free MoS_2 basal planes Co atoms bind exclusively at 3-fold hollow sites between surface atoms. A similar conclusion was reached theoretically by Raybaud et al.[17] for the case of the adsorption of Co atoms inside the van der Waals gap between MoS_2 layers. Their results indicate that the most stable configurations correspond to tetrahedral pseudointercalation followed by bulk tetrahedral intercalation. In both of these cases, the Co atom is 4-fold coordinated by sulfur atoms and has one molybdenum neighbor, similar to the adsorption at the 3F site described in this section. For the pseudointercalation and bulk tetrahedral intercalation configurations, the corresponding Co−S distances were found to be in the range of 2.14−2.22 Å (2.13−2.16 Å) whereas the Co−Mo distances have values around 2.69 Å (2.67 Å), respectively. These values are only slightly larger than those we have determined for the Ni atom adsorbed at the 3F site of 2.12 and 2.59 Å. The additional elongation seen for the

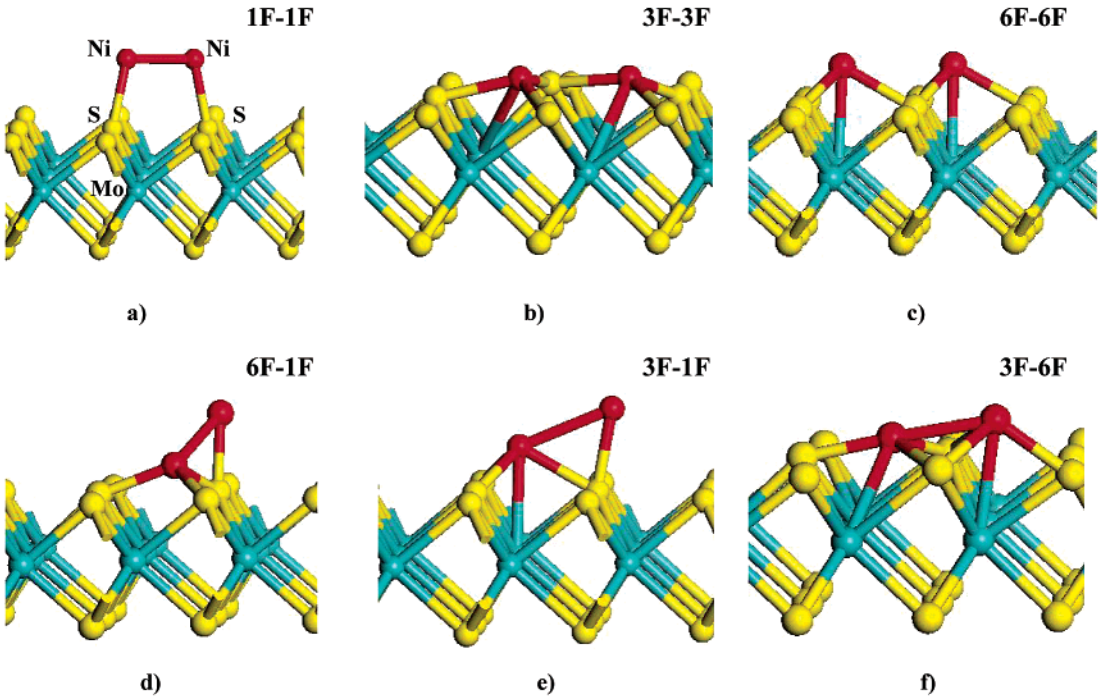

Figure 3. Pictorial views of the Ni dimers adsorbed at (a) 1F−1F sites, (b) 6F−6F sites, (c) 3F−3F sites, (d) 6F−1F, (e) 3F−1F sites, and (f) 3F−6F sites.

intercalation configurations is due to the additional interaction exercised by the neighboring MoS_2 slab on the metallic species Nevertheless, the increased stability of Co or Ni species when placed at sites above the Mo atom and 3-fold coordinated by sulfur atoms appears to be a common characteristic for either the basal plane or inside the van der Waals gap between these planes.

D2. Adsorption of Multiple Ni Atoms. Beside the adsorption of Ni atoms independently at various surface sites, we have also considered the possibility of having a simultaneous adsorption of Ni atoms at two or more surface sites. The characterization of these adsorption configurations is of increasing importance when the adsorption sites are closely separated and Ni atoms can interact with each other.

We have determined the adsorption configurations of two Ni atoms when they adsorb at the same type of neighboring sites, 1F−1F, 6F−6F, and 3F−3F, as well as the case when adsorption takes place at sites with different symmetries, namely, 1F−6F, 1F−3F, and 3F−6F. The corresponding configurations for these sets of structures are illustrated in Figure 3. The relative adsorption energies, E_{rel}, for these dimers as reported in Table 1 were determined with respect to the energy of a dimer adsorbed at neighboring 3F sites. We note that this 3F−3F reference state is only slightly more stable (by 0.4 kcal/mol per atom) than two isolated Ni atoms in 3F sites. This observation has been confirmed both by comparing the 3F−3F dimer with the analogous single Ni atom configurations and by performing calculations with two Ni atoms at nonadjacent 3F sites in our supercell. Although most of these pairs of adsorbed atoms lead to more-stable adsorption than the corresponding isolated adsorbates, the degree of stabilization varies considerably. The 3F−3F and 6F−6F pairs are stabilized by 0.4 and 1.2 kcal/mol per atom, respectively, relative to isolated adatoms in these same sites. The geometry of each Ni atom in these dimers is only slightly changed from that observed for an isolated adatom. The equivalent energy for the 1F−1F dimer is 12.6 kcal/mol per atom. In this case, the two Ni atoms practically form a new Ni−Ni dimer with a separation distance of d(Ni−Ni) = 2.24 Å (see Figure 3a). This separation is only 0.14 Å larger than the one we determined for an isolated Ni dimer in the gas phase. For the adsorption of Ni atoms at sites with different symmetries, we find that the 1F−6F and 1F−3F dimers are more stable than adsorption on the same sites as isolated atoms but that the 3F−6F dimer is less stable than the isolated adatoms. The main conclusions from this examination of possible Ni dimers is that the most stable dimer (3F−3F) has the two Ni atoms sitting in the same local environment as the most stable isolated adatom and that the interactions between the two Ni atoms are weak relative to the Ni−surface bonding. Although the stabilization of the 3F−3F dimer relative to the overall surface bonding is weak, it is sufficient to provide a considerable tendency for Ni atom clustering at the low temperatures used in the STM experiments of Weiss et al.[11]

To determine the effect of lateral interactions between the Ni atoms, we have also analyzed the variation of the binding energy per Ni atom with coverage for the case when adsorption takes place at the 3F sites. This dependence has been analyzed by considering up to nine Ni atoms in the 3-fold sites of our supercell such that coverages between $\theta = 0.11-1.0$ could be studied. Here, $\theta = 1.0$ means that the Ni adlayer contains one Ni atom per Mo atom in the surface trilayer. A simple row-by-row filling order has been considered in these studies. For example, at $\theta = {}^1/_3$, this construction gives an infinite row of Ni atoms on the surface. The lateral separation between the Ni−Ni atoms in adjacent 3F sites, 3.128 Å, is considerably larger than the Ni−Ni distance in an isolated Ni dimer (2.10 Å) or in bulk Ni (2.49 Å). We have characterized the energy of these configurations as a function of coverage in two ways. First, the total adsorption energy (E_{ads}) of the N adsorbed Ni atoms relative to N well-separated gas-phase Ni atoms is shown in Figure 5a. Second, we list in Table 1 the energy gained in moving from N isolated Ni atoms adsorbed in 3F surface sites to the coverage of interest, defined by

$$E_{ads,g} = [NE_1 - (N-1)E_0 - E_N]/N \qquad (2)$$

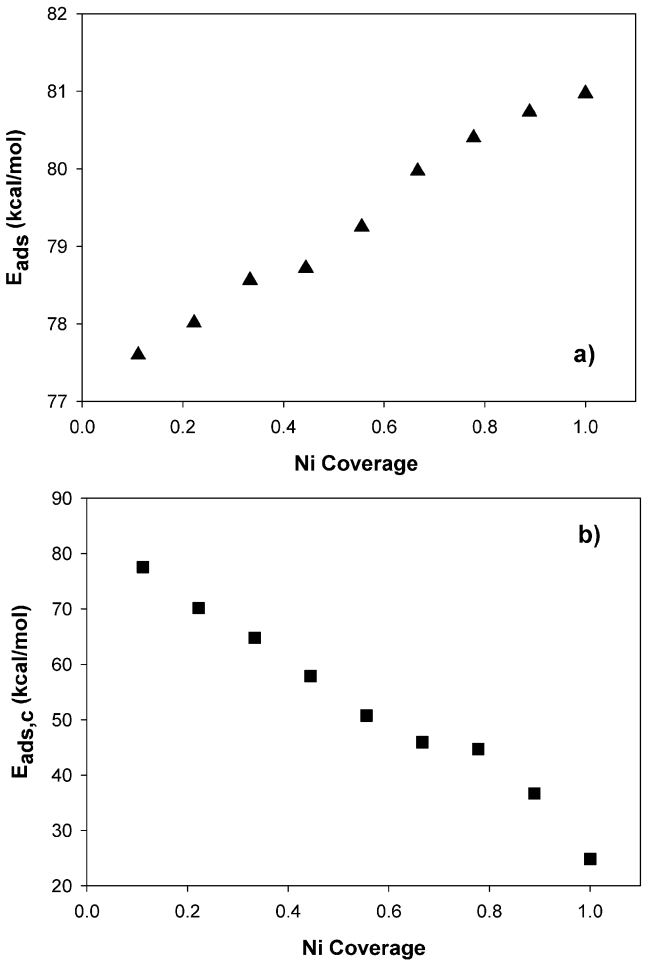

Figure 4. (a) Variation of the total binding energy (eq 1) and (b) the cluster adsorption energy $E_{c,ads}$ (eq 2) per Ni atom as function of coverage for the case of Ni adsorption at 3F surface sites.

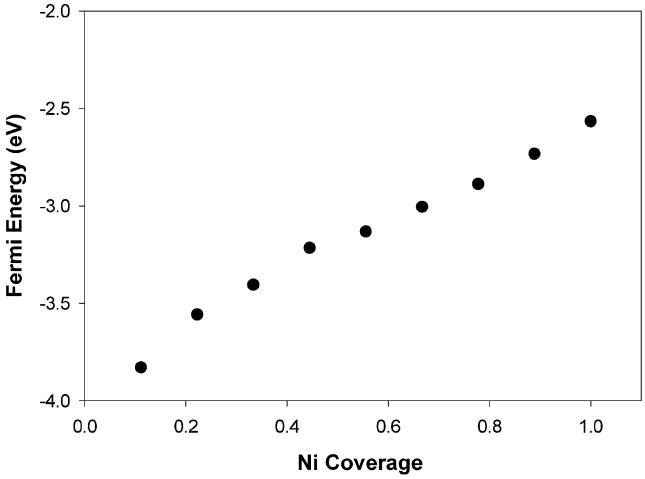

Figure 5. Variation of the Fermi energy as function of Ni coverage for the case of Ni adsorption at 3F sites on the MoS_2(0001) surface.

Here, E_N is the total energy of our computational supercell when N Ni atoms are adsorbed, and E_0 is the energy of the isolated slab. Both of these energies are reported on a per atom basis. Both measures of the adsorption energy clearly indicate that increasing the size of Ni clusters with all Ni atoms in 3F sites stabilizes the cluster with respect to the adsorption of isolated Ni atoms in 3F sites. This result is due to the attractive interactions between the Ni atoms as well as between these atoms and the MoS_2 surface. We also note (see data in Table 1) that as the coverage is increased from $^1/_9$ to 1 the vertical separation between Ni and surface Mo atoms increases from 2.591 to 2.767 Å. This effect indicates the trend of Ni atoms to separate from the surface as Ni clusters form. Similar behavior for the height of metal clusters above a surface as a function of coverage has been observed in studies of transition metals on metal oxide surfaces.[40]

To attempt to describe the binding energy of Ni clusters as a single unit with the MoS_2 surface, we calculated the cluster adsorption energy per Ni atom defined as

$$E_{ads,c} = \{E_{clust} + E_{slab} - E_{(clust+slab)}\}/N \qquad (3)$$

where E_{clust} is the total energy of the cluster containing N atoms of Ni, E_{slab} is the total energy of the slab in the absence of the adsorbate, and $E_{(clust+slab)}$ is the total energy of the cluster/slab system. The cluster energy E_{clust} above has been determined by relaxing the atomic coordinates in the direction perpendicular to the slab direction (z axis) but freezing the atomic motion along the x and y directions to maintain the lateral configuration seen on the surface. This quantity is closely related to the work of separation, a quantity that has been used to assess the adhesion strength of heteroepitaxial films.[40] The variations of $E_{ads,c}$ as function of Ni coverage are shown in Figure 4b. The cluster binding energy per Ni atom decreases strongly with coverage. That is, increases in Ni coverage lead to enhanced overall adsorption energy because of stabilizing Ni−Ni interactions, as mentioned in our discussion above of the total adsorption energy per atom, but these lateral interactions significantly decrease the interaction between the Ni cluster and the surface when the cluster is viewed as a single, cohesive unit.

The increase of Ni coverage on the MoS_2(0001) surface also has significant effects upon the electronic properties of the system. For example, we present in Figure 5 the variation of the Fermi level as function of the Ni coverage when adsorption takes place at the 3F site. As can be seen in this Figure, there is a continuous shift upward of the Fermi level with Ni coverage toward the vacuum level taken as zero energy.

Papageorgopoulos and Kamaratos[41] have shown experimentally that below room temperature the deposition of Ni on the basal plane of MoS_2 leads to the formation of small islands followed by a change to 3D particles upon heating at 450 K. Moreover, the increase of temperature leads to a decrease of the sticking coefficient of Ni atoms, an effect attributed to the formation of islands and particles. In the regime of lower coverages where Ni adsorbs directly to the surface, it was determined that initially there is a linear decrease of the work function of about 0.26 eV. This work function dependence becomes nonlinear for increasing coverage because of island formation. From the data in Figure 5, we can observe that if the deposition of Ni atoms takes place in a regular pattern at 3F sites then there will be an upward shift of the Fermi level with a dependence of coverage that is almost linear up to $\theta = {}^1/_3$. As a result of this shift, there will be a decrease of the work function, in agreement with experimental data.[41]

In Figure 6, we represent the variation of the total DOS for the Ni−MoS_2 system as function of the coverage of Ni atoms adsorbed at 3F sites. Our calculations indicate that despite a continuous decrease of the band gap the system remains nonmetallic even in the case when Ni atoms occupy all 3-fold sites available on the surface. The lack of metallic character observed here has also been observed experimentally by Papageorgopoulos and Kamaratos.[41]

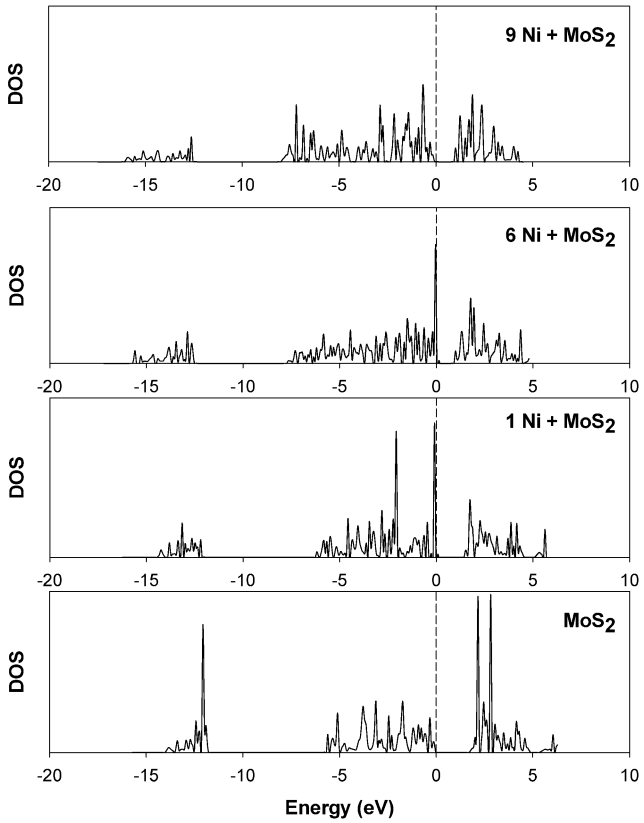

Figure 6. Variation of the total DOS as function of Ni coverage when adsorption takes place at 3F sites on the MoS_2(0001) surface. In each DOS, the zero energy is taken to be at the Fermi level.

There are of course many structures in which Ni clusters can potentially form on the surface. We have examined several geometries that correspond to isolated Ni clusters to complement the surface-filling calculations described above. The corresponding clusters that are analyzed are represented in Figure 7. The first types correspond to triangular Ni_3 clusters with their planes oriented perpendicular and parallel, respectively, to the surface. In the first case, the binding to the surface takes place through a Ni atom positioned at the 3F site whereas in the second case the adsorption takes place on top of S sites (1F configurations). The corresponding binding energies per Ni atom are 60.4 and 19.7 kcal/mol, respectively. These values are clearly smaller than the corresponding energies found for the individual Ni atoms adsorbed at 3F and 1F sites of 77.5 and 33.8 kcal/mol, respectively. The increase of the size of the cluster from Ni_3 to Ni_4 for the case when adsorption takes place on top of S atoms leads to an even larger decrease of the adsorption energy per Ni atom to 16 kcal/mol. These results imply that none of the clusters shown in Figure 7 are more stable than having the same Ni atoms adsorbed in adjacent 3F positions as discussed above.

Similar conclusions have been obtained for the analysis of even larger clusters. In particular, we have considered the adsorption of Ni_7 clusters. These clusters are composed of a central Ni atom surrounded by six other Ni atoms distributed in a regular hexagonal configuration at about 60° relative to the central atom. For these clusters, we have considered the adsorption of the central atom at either a 6F or a 3F site, respectively (see Figure 7d and e). The central 6F atom is surrounded by three atoms positioned at 3F sites and three atoms at 1F sites. The cluster centered on a 3F atom contains three Ni atoms at 6F sites and three atoms at 1F sites. The corresponding adsorption energies of these clusters were only 9.5 and 10.2 kcal/mol per Ni atom, respectively. As with the Ni_3 and Ni_4 clusters described above, these Ni_7 clusters are considerably less stable than the adsorption of the same number of Ni atoms in adjacent 3F sites.

D3. Diffusion of Ni Atoms on MoS_2(0001). An additional set of investigations has been dedicated to the evaluation of the minimum-energy paths for the diffusion of the Ni atom between different adsorption configurations on the MoS_2(0001)

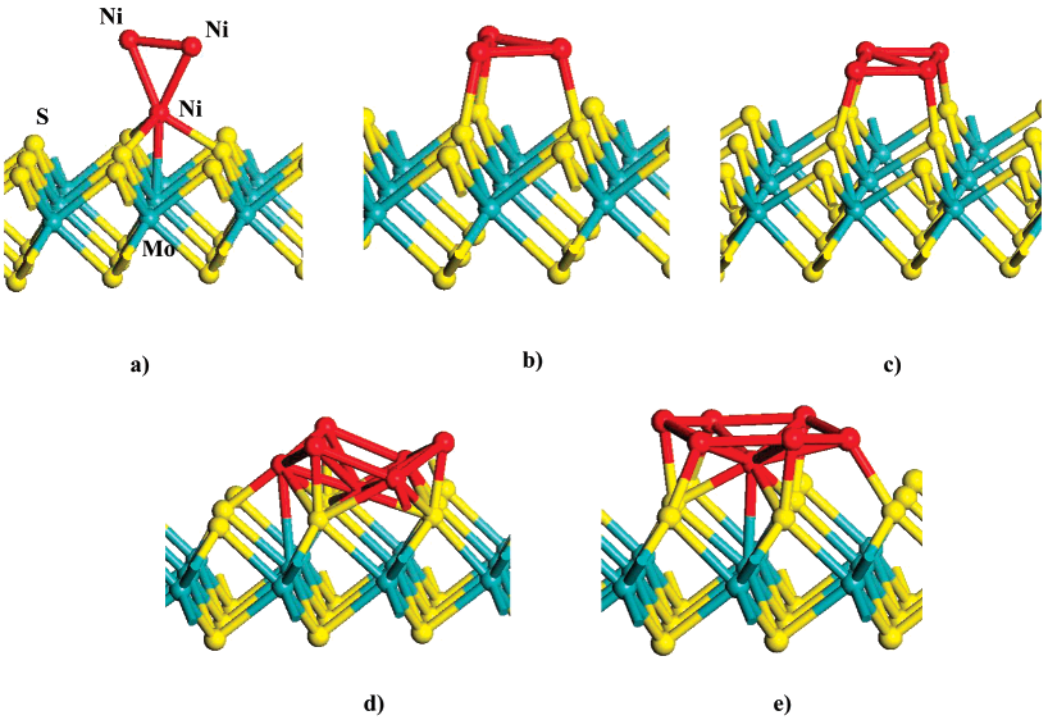

Figure 7. Pictorial view of the Ni_3, Ni_4, and Ni_7 clusters investigated in the present work. Plot (a) corresponds to a cluster with one Ni atom bonded to a 3F site and the other two in a vertical plane perpendicular to the surface; configurations (b) and (c) correspond to Ni_3 and Ni_4 clusters bonded on top of S atoms; and plots (d) and (e) represent Ni_7 clusters centered around a 6F and 3F sites, respectively.

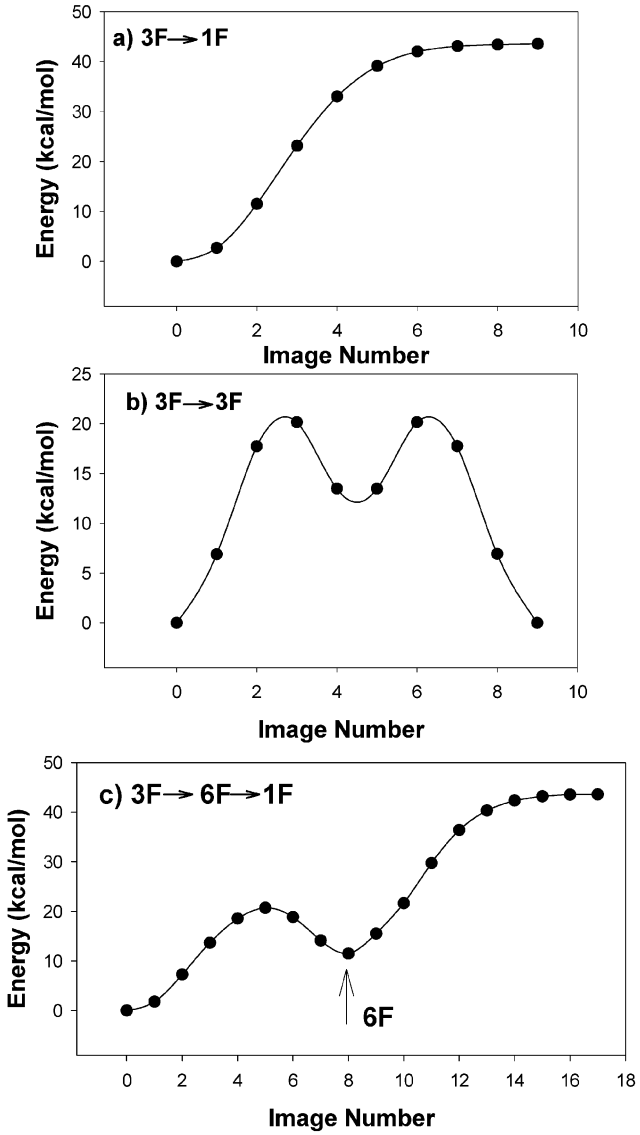

Figure 8. Potential energy surface for the diffusion of Ni atoms along the following pathways: (a) 3F → 1F, (b) 3F → 6F → 3F, and (c) 3F → 6F → 1F.

surface. These calculations have been performed using the NEB method.[31] We have considered three diffusion pathways suggested by the surface symmetry: 3F → 1F, 3F → 6F → 3F, and 3F → 6F → 1F. The minimum-energy paths corresponding to these processes are represented in Figure 8. As can be seen from this Figure, our calculations indicate that among the set of three diffusion pathways considered here the 3F → 6F → 3F path has the smallest barrier, with a value of 20.1 kcal/mol.

We have also considered the case of Ni diffusion from 3F → 6F sites when a second Ni atom is positioned at a nearby 3F site. In this case, the calculated diffusion barrier decreases only slightly relative to the barrier obtained for the diffusion of a single Ni atom. This result indicates that the stabilization provided by the neighboring Ni atom positioned at the 3F site upon the diffusing atom is small.

Another important finding that is apparent from the potential profiles for 3F → 1F and 6F → 1F diffusion pathways is that adsorption at the 1F site does not correspond to a local minimum but to a saddle point. We have analyzed in more detail the potential region around the 1F adsorption site and find that in this region the potential is very flat. For example, by changing the angle formed by the S−Ni bond with the surface normal from 0 to 14 or 23° and relaxing all the other degrees of freedom, we have determined that the total potential decreases by 0.2 and 1.9 kcal/mol, respectively, relative to the vertical adsorption configuration of Ni on top of a S atom.

Our results indicate that in the low-temperature regime the diffusion rates of individual atoms via the three pathways we have considered are extremely small. If we assume that individual Ni atoms attempt to hop over the barriers observed in our pathways with an attempt frequency of 10^{13} s^{-1}, then the hopping frequency drops from roughly 0.02 s^{-1} at room temperature to 10^{-9} s^{-1} at 200 K. This result is dramatically different from the rapidly diffusing surface species observed via STM by Weiss et al.,[11] who report that the observed Ni species hop on submicrosecond time scales at 77 K and room temperature. Assuming the same attempt frequency as above requires an energy barrier of approximately 2.5 kcal/mol for hopping to occur once per microsecond at 77 K.

One way to compare the energy barriers for diffusion mentioned above to other systems where surface diffusion has been quantified is to examine the ratio of the diffusion activation energy to the energy required for desorption. Our DFT results predict that this ratio is 0.26. Using the same desorption energy (77 kcal/mol) but the energy barrier estimated above from the experimental observations of Weiss et al.[11] (2.5 kcal/mol) yields a ratio of 0.03. Reviewing experimental measurements of this ratio for the diffusion of metal and alkali atoms on metal surfaces, Gomer found that most data lies in the range of 0.07−0.2, although examples as low as 0.03 and as high as 0.30 are known.[42] Unfortunately, similar data for metal atom diffusion on nonmetallic surfaces is not currently available. We can draw only a relatively weak conclusion from this discussion: neither our DFT results nor the experimental results of Weiss et al.[11] yield diffusion barriers that are unprecedented when compared with the desorption energy of the diffusing atom. We discuss the possible sources of the discrepancy between our DFT-based predictions and experimental observations further below.

E. Adsorption of Thiophene Molecules on a Bare Basal Surface and on a Surface with Adsorbed Ni Species. As thiophene is one of the representative molecules involved in the desulfurization processes, it is interesting to analyze the chemisorption properties of this molecule on the MoS_2 basal plane and the role played by the adsorbed Ni species upon these properties.

In the case of the adsorption of thiophene on the bare surface, we find very small adsorption energies, indicating a physisorption mechanism. This result is in agreement with previous experimental findings determined by Salmeron et al.[13] on the basis of TPD investigations or the data obtained by Rodriguez et al.[14] using synchrotron-based high-resolution photoemission. Similar weak interactions of thiophene with MoS_2 model clusters were determined on the basis of ab initio SCF calculations by Rodriguez.[15] In the context of HDS, it is useful to note that these weak binding energies imply extremely short residence times of thiophene on the MoS_2 basal plane.

For the case of the surface with adsorbed Ni species, we have analyzed the adsorption of thiophene on top of the Ni atom positioned at the 3F site. We considered two adsorption configurations of thiophene, both with binding of the molecule to the Ni atom via the S atom in the molecule (see Figure 9). The first configuration placed the aromatic ring perpendicular to the surface. The second configuration has the aromatic ring tilted with respect to the surface plane. Our results (see Table 1) indicate that the S atom in thiophene adsorbs at about 2.2 Å above the Ni atom. Both the vertical and tilted configurations

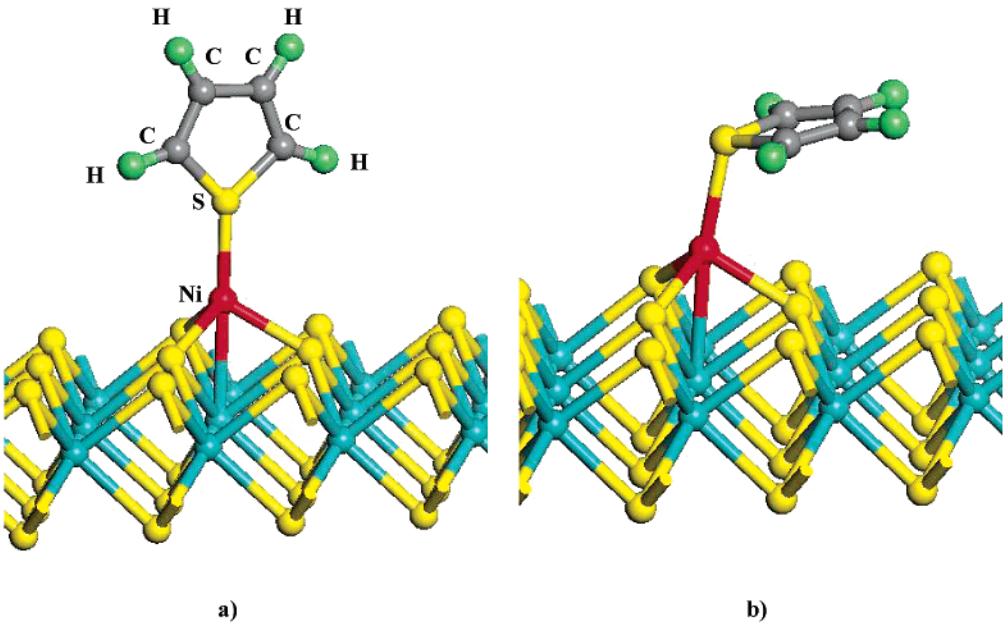

Figure 9. (a) Vertical and (b) tilted adsorption configurations of thiophene on Ni atoms adsorbed at 3F sites on the MoS_2 basal plane.

have similar adsorption energies, with a slightly larger binding energy for the adsorption in the tilted configuration. The binding energy we consider here is the energy required to desorb thiophene from the surface molecularly, leaving the Ni atom on the surface. As these energies are significantly larger than those of thiophene adsorbed on the bare surface, it follows that one role played by adsorbed Ni atoms on MoS_2 basal planes is to increase the binding energy and hence the residence time of thiophene on the surface. A similar conclusion has been obtained experimentally by Rodriguez et al.[14] Photoemission spectra of thiophene adsorbed on $Ni_{1.3}/MoS_x$ and $Ni_{2.6}/MoS_x$ systems indicated that the addition of Ni enhances the adsorption energy of thiophene by at least 5−10 kcal/mol relative to the case when adsorption takes place on the pure MoS_x surface.

F. Diffusion of the Ni−Thiophene Complex on the MoS_2-(0001) Surface. Besides increasing the binding of thiophene to the surface, Kushmerick et al.[11] have suggested a possible second role for the Ni promoter on MoS_2 basal planes. They suggested that Ni−thiophene complexes may be highly mobile on MoS_2 basal planes, allowing these complexes to transport thiophene or other sulfur-containing hydrocarbons efficiently to catalytically active sites positioned at MoS_2 sheet edges or defects. In light of this proposed phenomenon, it is interesting to examine the barrier to diffusion for the Ni−thiophene complex described above.

We have determined the diffusion barrier for the Ni−thiophene complex using the NEB method as described in previous sections for the case of a pathway between two neighboring 3F and 6F sites. In this case, we have considered only the tilted bonding configuration of thiophene to the Ni atom. The initial diffusion path has been taken by linear interpolation between the two minimum-energy states in adjacent 3-fold sites. The corresponding minimum-energy path is represented in Figure 10. As can be seen from this Figure, the barrier for diffusion is relatively large, with a value of about 21 kcal/mol. This value is not surprising in light of the diffusion barriers reported above for isolated Ni atoms. Indeed, it is apparent that the diffusion barrier encountered by the Ni−thiophene complex is largely due to the energy required to move the Ni atom across the surface. On the basis of this activation

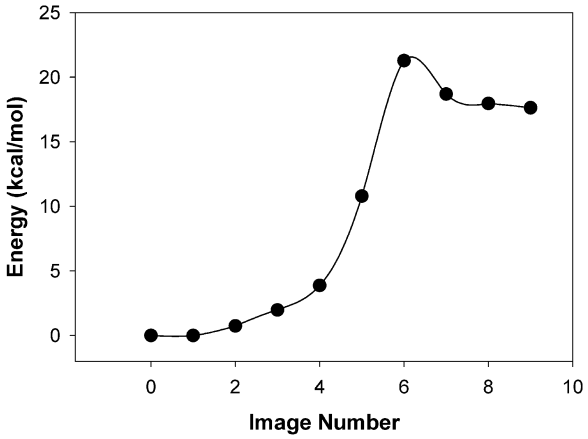

Figure 10. Potential energy surface for the diffusion of the Ni−thiophene complex along the 3F → 6F pathway.

energy, it appears that the diffusion of the Ni−thiophene complex considered here is negligibly slow at low temperatures.

G. Adsorption of Ni Atoms and the Ni−Thiophene Complex at Sulfur Defect Sites. The characterization of the chemisorption of Ni atoms and Ni−thiophene complexes on the defective MoS_2 basal plane is the final topic considered in the present work. As has been shown experimentally by Kushmerick et al.,[11] defective sites are observed on this surface in the regime of low temperatures. In this case, the defects were assigned from STM images as single S vacancies on the MoS_2 surface. A primary effect of these defects was to stabilize Ni atoms adsorbed on the surface. For example, it was shown that the increase in the binding energy of Ni atoms or clusters at these S vacancies made it impossible to displace the Ni atoms using the STM probe tip.[11]

We analyzed the adsorption of a single Ni atom at a S vacancy on a MoS_2(0001) surface using the same supercell as in our previous calculations. The S vacancy was made by simply removing one S atom from the top S layer in the surface. The geometry of the Ni atoms and all of the surface atoms was fully relaxed in our calculations. Independent of the initial position of the Ni atom around the vacancy, either on top or in a neighboring 3F or 6F site, the final adsorption position corre-

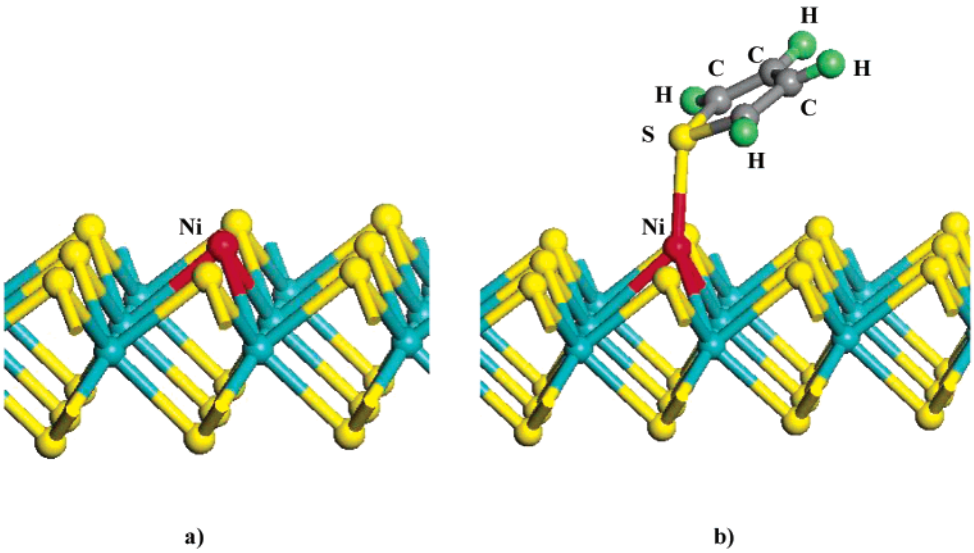

Figure 11. Pictorial view of (a) Ni and (b) the Ni−thiophene complex adsorbed on the defective MoS_2(0001) surface.

sponds to a Ni atom filling the S vacancy (see Figure 11a). For this configuration, we have determined an adsorption energy of 98.5 kcal/mol using ultrasoft pseudopotentials (USP) or 102.3 kcal/mol using the PAW method. These adsorption energies are roughly 20 kcal/mol larger than those we find for isolated Ni atoms on defect-free basal planes (see Table 1). These results support the experimental findings[14] that S vacancies significantly increase the binding energy of Ni atoms to the surface, leading to a very stable adsorption configuration.

We have also tested the modification of the binding energy of thiophene when it is adsorbed on Ni atoms that fill the S vacancies (see Figure 11b). In this case, the corresponding thiophene adsorption energies were 15.2 kcal/mol using USPs and 14.7 kcal/mol using the PAW method. These values are about 5 kcal/mol smaller than those determined when the Ni−thiophene complex sits on an undefective surface. On the basis of these results, it can be concluded that defective sites present on the surface serve as strong centers for Ni stabilization. As on defect-free basal planes, thiophene molecules bind to these stabilized Ni atoms much more strongly than they do to the bare basal plane, although the binding energy of thiophene to these defect-site Ni atoms is somewhat lower than the corresponding binding energy for Ni on defect-free MoS_2(0001).

H. Comparison with STM Experiments. The most puzzling feature of our results is their apparent contradiction of the experimental conclusions drawn by Weiss et al.[11] regarding the diffusion of Ni atoms on MoS_2 basal planes. Our calculations indicate that if isolated Ni atoms diffuse via direct hopping between stable adsorption sites on the surface then an energy barrier of at least 20 kcal/mol must be overcome. This energy barrier would render Ni atoms essentially stationary on the timescale of STM imaging in the experiments of Weiss et al. at 77 K. However, STM experiments at this temperature were unable to image localized Ni atoms. We conclude by considering two scenarios that could potentially explain this discrepancy. It is possible that Ni does not diffuse on the surface by a direct hopping mechanism, that is, by a mechanism in which essentially only the Ni atom moves. It is well known, for example, that metal atom diffusion on (100) transition-metal surfaces can proceed via substitution mechanisms in which the diffusing atom moves into the surface layer, displacing another atom onto the surface.[43,44] This scenario seems unlikely in view of the strong bonding between individual atoms in the MoS_2 surface. Moreover, when a Ni atom was manipulated with an STM tip at 4 K, it was seen to remain on top of the surface at all times as the atom "diffuses" across many lattice sites.[11] We also note that although surface atoms were allowed to relax fully in our DFT calculations only small relaxations of the top-layer S atoms were observed as Ni diffused between stable adsorption sites. Thus, although our calculations cannot unequivocally exclude the existence of some concerted diffusion mechanism that leads to single Ni atoms diffusing with very small energy barriers, this possibility does not seem likely.

A second scenario is that the rapidly diffusing species observed by Weiss et al.[11] at 77 K and room temperature are not individual Ni atoms. For this scenario to be consistent with our results, the rapidly diffusing species should include essentially all of the surface Ni since no stable Ni atoms or clusters were observed experimentally except at 4 K. Weiss et al.[11] report that at 4 K clusters of Ni are less susceptible to being moved by an STM tip than individual Ni atoms. We note, however, that Ni clusters could possibly diffuse via stepwise mechanisms with low energy barriers, even though the energy required to move the entire cluster in a concerted manner may be large.[45] If this occurs, then clusters that can diffuse readily on the surface could still be difficult to move with an STM tip. STM experiments examining Co clusters on MoS_2 basal planes have shown that Co clusters undergo substantial shape changes over time,[12] although similar results have not been reported during equivalent experiments with Ni on MoS_2.[11] We have directly examined the influence of adjacent Ni atoms on the diffusion activation energy of single Ni atoms and have found this influence to be very small. Our calculations with a variety of Ni clusters indicate that Ni adsorbs most favorably in adjacent 3F sites. This observation, coupled with the large activation energy observed for the diffusion of one Ni atom in a 3F−3F dimer, does not suggest that the existence of low-energy diffusion paths for small Ni clusters in 3F sites is likely. Further investigations of the possibility of mobile Ni clusters will require the construction of specific diffusion pathways using DFT or the direct imaging of cluster motions experimentally.

It is also possible that the rapidly diffusing species observed by Weiss et al.[11] are adsorbed Ni atoms decorated by heteroatoms that they have abstracted from the surface or from contaminants in the experimental system. We are currently performing DFT calculations examining the adsorption and diffusion of NiS_x and NiH_x complexes on MoS_2 basal planes. Our preliminary results indicate that whereas some of these

complexes have lower diffusion activation energies than individual Ni atoms these reduced energies are still quite large when compared to those inferred from the STM experiments of Weiss et al. We will report in detail on these results in the future.

For completeness, we must consider one additional possibility: that plane wave DFT is grossly inaccurate for Ni adsorption on MoS_2. The accuracy of DFT for surface calculations has recently been carefully discussed by Feibelman et al.,[46] for example, where carefully converged DFT calculations yield results that are different from experimental measurements, namely, the sitting of CO on Pt(111). These authors point out that whereas adsorption energies computed using DFT may be in error at the level of tenths of an electronvolt, it is generally expected that energy barriers determined for processes involving smaller perturbations of the physical structure (e.g., surface diffusion) exhibit lower levels of inaccuracy compared to reality. Since the difference between the DFT and observed diffusion activation barriers under consideration here is on the order of 1 eV, it seems unlikely that this difference can be accounted for by systematic inaccuracy in density functional theory. We emphasize that we have taken steps similar to those in the work of Feibelman et al.[46] to ensure that the central conclusions of our DFT calculations are consistent among separate calculations with different treatments of core electrons, including ultrasoft pseudopotentials and the projector augmented wave method.

None of the scenarios outlined above currently provides an unambiguous resolution to the puzzle of identifying the rapidly diffusing species observed in STM experiments of Ni-covered MoS_2 basal planes. It is our hope that the DFT-based calculations we have presented here will spur further experimental and theoretical work on this issue.

Conclusions

We have used plane wave DFT to examine the adsorption and diffusion of Ni atoms, Ni clusters, and Ni−thiophene complexes on MoS_2(0001). Our main results can be summarized as follows:

(a) There are several locally stable adsorption configurations of isolated Ni atoms on the MoS_2 basal plane. The most stable site is when Ni sits in the surface 3-fold site with an adsorption energy of about 77 kcal/mol.

(b) Ni clusters bind most favorably to the surface when all Ni atoms are in adjacent 3-fold sites. The additional adsorption energy created by Ni−Ni interactions in clusters of this type is sufficient to make Ni clustering favorable at temperatures below room temperature.

(c) In the case of Ni adsorption at 3-fold sites, there is a continuous shift of the Fermi level to the vacuum level as a function of coverage. This process takes place with a corresponding decrease of the band gap with coverage, but the system remains nonmetallic even when Ni atoms occupy all of the 3-fold sites.

(d) By assuming a direct hopping mechanism for Ni surface diffusion, we have evaluated the diffusion barriers for Ni atoms between different adsorption sites. Our results indicate diffusion barriers in excess of 20 kcal/mol.

(e) Adsorbed Ni species significantly increase the binding energy of the thiophene molecule to the surface to about 20.1 kcal/mol. This result supports the previous experimental findings that one role of these metallic species is to increase the binding energy and residence time of the thiophene molecule on the surface.

(f) We find an activation energy of about 21 kcal/mol for the diffusion of a Ni−thiophene complex between adjacent 3-fold sites. This indicates that at temperatures below room temperature individual Ni atoms cannot transport thiophene molecules on the surface.

(g) When present on the surface, S vacancies act as stabilization centers for Ni atoms. The adsorption energy of Ni at these sites was found to be about 21 kcal/mol higher than the most stable adsorption configuration on a nondefective surface. In contrast, thiophene is less strongly bound by about 5 kcal/mol to Ni atoms adsorbed at the defect site relative to the case when Ni is adsorbed on the defect-free surface.

Acknowledgment. We gratefully acknowledge the supercomputer allocation provided by the Pittsburgh Supercomputer Center under the SC^2 partnership program. D.S.S. is an ORISE Faculty Fellow at NETL and an Alfred P. Sloan fellow.

References and Notes

(1) United States Environmental Protection Agency; EPA's Program for Cleaner Vehicles and Cleaner Gasoline, EPA420-F-99-051, December 1999 (http://www.epa.gov/otaq/regs/ld-hwy/tier-2/f99051.htm).

(2) Topsøe, H.; Clausen, B. S.; Franklin, F. E.; Massoth, E. In *Science and Technology in Catalysis: Hydrotreating Catalysis*; Anderson, J. R., Boudart, M., Eds.; Springer: Berlin, 1996; Vol. 11.

(3) Kabe, T.; Ishihara, A.; Qqian, W. In *Hydrodesulfurization and Hydrogenation*; Wiley: New York, 1999.

(4) Prins, R.; De Beer, V. H. J.; Somorjai, G. A. *Catal. Rev.—Sci. Eng.* **1989**, *31*, 1.

(5) Byskov, L. S.; Nørskov, J. K.; Clausen, B. S.; Topsøe, H. *J. Catal.* **1999**, *187*, 109.

(6) Helveg, S.; Lauritsen, J. V.; Lægsgaard, S.; Stensgaard, I.; Nørskov, J. K.; Clausen, B. S.; Topsøe, H.; Besenbacher, F. *Phys. Rev. Lett.* **2000**, *84*, 951.

(7) Lauritsen, J. V.; Helve, Lægsgaard, S.; Stensgaard, I.; Clausen, B. S.; Topsøe, H.; Besenbacher, F. *J. Catal.* **2001**, *197*, 1.

(8) Kasztelan, S.; Toulhoat, H.; Grimblot, J.; Bonnelle, J. P. *Appl. Catal.* **1984**, *13*, 127.

(9) Raybaud, P.; Hafner, J.; Kresse, G.; Toulhoat, H. *Phys. Rev. Lett.* **1998**, *80*, 1481.

(10) Kushmerick, J. G.; Weiss, P. S. *J. Phys. Chem. B* **1998**, *102*, 10094.

(11) Kushmerick, J. G.; Han, K. P.; Johnson, J. A.; Weiss, P. S. *J. Phys. Chem. B* **2000**, *104*, 2980.

(12) Kandell, S. A.; Weiss, P. S. *J. Phys. Chem. B* **2001**, *105*, 8102.

(13) Salmeron, M.; Somorjai, G. A.; Wold, A.; Chianelli, R.; Liang K. S. *Chem. Phys. Lett.* **1982**, *90*, 105.

(14) Rodriguez, J. A.; Dvorak, J.; Capitano, A. T.; Gabelnick, A. M.; Gland, J. L. *Surf. Sci.* **1999**, *429*, L462.

(15) Rodriguez, J. A. *J. Phys. Chem B* **1997**, *101*, 7524.

(16) Raybaud, P.; Hafner, J.; Kresse, G.; Toulhoat, H. *Surf. Sci.* **1998**, *407*, 237.

(17) Raybaud, P.; Hafner, J.; Kresse, G.; Kasztelan, S.; Toulhoat, H. *J. Catal.* **2000**, *190*, 128.

(18) Raybaud, P.; Hafner, J.; Kresse, G.; Kasztelan, S.; Toulhoat, H. *J. Catal.* **2000**, *189*, 129.

(19) Schweiger, H.; Raybaud, P.; Kresse, G.; Toulhoat, H. *J. Catal.* **2002**, *207*, 76.

(20) Kresse, G.; Hafner, J. *Phys. Rev. B* **1993**, *48*, 13115.

(21) Kresse, G.; Furthmüller, J. *Comput. Mater. Sci.* **1996**, *6*, 15.

(22) Kresse, G.; Furthmüller, J. *Phys. Rev. B* **1996**, *54*, 11169.

(23) Perdew, J. P.; Chevary, J. A.; Vosko, S. H.; Jackson, K. A.; Pedersen, M. R.; Singh, D. J.; Frolhais, C. *Phys. Rev. B* **1992**, *46*, 6671.

(24) Vanderbilt, D. *Phys. Rev. B* **1990**, *41*, 7892.

(25) Kresse, G.; Hafner, J. *J. Phys.: Condens. Matter* **1994**, *6*, 8245.

(26) Monkhorst, H. J.; Pack, J. D. *Phys. Rev. B* **1976**, *13*, 5188.

(27) Blöch, P. E. *Phys. Rev. B* **1994**, *50*, 17953.

(28) Kresse, G.; Joubert, D. *Phys. Rev. B* **1999**, *59*, 1758.

(29) Methfessel, M.; Paxton, A. T. *Phys. Rev. B* **1989**, *40*, 3616.

(30) Kresse, G.; Hafner, J. *Phys. Rev. B* **1993**, *47*, 558.

(31) Mills, G.; Jónsson, H.; Schenter, G. K. *Surf. Sci.* **1995**, *324*, 305.

(32) Bronsema, K. D.; De Boer, J. L.; Jellinek, F. *Z. Anorg. Allg. Chem.* **1986**, *540*, 15.

(33) Raybaud, P.; Kresse, G.; Hafner, J.; Toulhoat, H. *J. Phys.: Condens. Matter* **1997**, *9*, 11085.

(34) Harshbarger, W. R.; Bauer, S. H. *Acta Crystallogr., Sect B* **1970**, *26*, 1010.

(35) Bak, B.; Christensen, D.; Hansen-Nygaard, L.; Rastrup-Andersen, J. *J. Mol. Spectrosc.* **1961**, *87*, 58.

(36) Moroni, E.; Kresse, G.; Hafner, J.; Furtmüller, J. *Phys. Rev. B* **1997**, *56*, 15629.
(37) Mittendorfer, F.; Hafner, J. *Surf. Sci.* **2001**, *492*, 27.
(38) Feibelman, P. J. *Science* **2002**, *295*, 99.
(39) Hirschl, R.; Hafner, J. *Surf. Sci*. **2002**, *498*, 37.
(40) Asthagiri, A.; Sholl, D. S. *J. Chem. Phys*. **2002**, *116*, 9914.
(41) Papageorgopoulos, C.; Kamaratos, M. *Surf. Sci*. **1985**, *164*, 353.
(42) Gomer, R. *Rep. Prog. Phys*. **1990**, *53*, 917.
(43) Kellogg, G. L.; Feibelman, P. J. *Phys. Rev. Lett*. **1990**, *64*, 3143.
(44) Feibelman, P. J.; Stumpf, R. *Phys. Rev. B* **1999**, *59*, 5892.
(45) Sholl, D.; Skodje, R. T. *Phys. Rev. Lett.* **1995**, *75*, 3158.
(46) Feibelman, P. J.; Hammer, B.; Norskov, J. K.; Wagner, F.; Scheffler, M.; Stumpf, R.; Watwe, R.; Dumesic, J. *J. Phys. Chem*. *B* **2001**, *105*, 4018.